The Astrophysical Journal, 674:576–585, 2008 February 10

CORONAL MASS EJECTION–ASSOCIATED CORONAL DIMMINGS

A. A. Reinard
University of Colorado/Cooperative Institute for Research in Environmental Sciences and National Oceanic and Atmospheric Administration/Space Weather Prediction Center, Boulder, CO

and

D. A. Biesecker
National Oceanic and Atmospheric Administration/Space Weather Prediction Center, Boulder, CO
Received 2007 February 22; accepted 2007 October 18

ABSTRACT

We report on a statistical analysis of 96 CME-associated EUV coronal dimmings between 1998 and 2000. We investigate the size and location of the events and characterize how these events evolve with time. The durations typically range from 3 to 12 hr. The dimmings appear most frequently within the belt of active regions (20°–50° latitude). Dimming events are generally symmetric in latitude and longitude with some tendency to be broader in latitude. The temporal profiles of most events are characterized by a sharp rise and a gradual recovery. Although the majority of cases are well fit by a single recovery slope, a large minority of events have a two-part decay with an initial decaying slope that is similar in magnitude to the rising slope and a secondary, flatter, decay lasting several hours.

Subject headings: Sun: activity — Sun: corona — Sun: coronal mass ejections (CMEs)

1. INTRODUCTION

Coronal dimmings, also called transient coronal holes or depletions, are regions in the low corona consisting of reduced emission in white light, extreme-ultraviolet (EUV), and soft X-rays (Hansen et al. 1974; Stewart & McCabe 1974; Rust & Hildner 1976; Sterling & Hudson 1997; Thompson et al. 1999, 2000; Gopalswamy & Hanaoka 1998). These dimmings often appear in conjunction with coronal mass ejections (CMEs) and are considered a low coronal signature of CMEs. A few studies with a limited sample size indicate that dimming position angles (P.A.s) compare well with the associated CME P.A.s (e.g., Harrison et al. 2003; Thompson et al. 2000). In general, the locations of the dimmings appear to be closely aligned with the apparent footpoint or footpoints of a CME (Thompson et al. 2000) and dimmings are closely associated in time with the onset of CMEs (Hudson & Webb 1997 and references therein).

The reduced emissions in the corona, characteristic of dimmings, can be explained by mass loss or by temperature variations. Multiwavelength observations of dimming regions indicate that the drop in emission in one wavelength is not accounted for by an increase in another wavelength, and often all observable wavelengths drop in emission at the same time (Harrison & Lyons 2000). Thus, temperature variations cannot account for all, or even most, of the darkening observed. Further, Harra & Sterling (2001) studied Doppler observations within the dimming and concluded that the dimming material is indeed flowing outward. Studies vary on the exact quantity of mass lost from a dimming event, but most results indicate that between 10% and 100% of the CME mass is accounted for by the mass evacuated from the dimming (e.g., Harrison & Lyons 2000; Hudson et al. 1998).

Typical timescales for dimmings range from several hours to several days, although most disappear within a day (Thompson et al. 2000; Zarro et al. 1999). The intensities of these dimmings can become as dark as coronal holes, although not all reach intensities that low (Thompson et al. 2000). Dimmings disappear through some combination of constant recovery of intensity throughout the dimming and contraction at their boundaries, although some events have been reported to expand behind the associated EIT wave (Kahler & Hudson 2001; Podladchikova & Berghmans 2005, and references therein). Dimmings often occur in two roughly symmetric locations at the footpoints of pre-CME sigmoid structures (e.g., Sterling & Hudson 1997; Hudson et al. 1998).

Coronal dimmings offer a look into the details of the magnetic processes that occur during a CME. The full characterization of the spatial and temporal properties of these dimmings, therefore, has the potential to directly affect our understanding of CME initiation, and may have further implications for the resulting CME properties such as mass, velocity, and density. The results described above were derived from studies with a handful of events. At this point, our knowledge has advanced sufficiently that there is a need for a larger statistical sample to more fully characterize the general spatial and temporal structure of dimmings. In this paper we describe a statistical study of the characteristics of CME-associated coronal dimmings from 1998 to 2000. This information will be key to understanding the dynamics of dimming events and how they relate to CMEs, including how well certain dimming characteristics are related to subsequent CME characteristics. The results have implications for space weather predictions as well as understanding of CME processes. The paper is organized as follows. In § 2 we describe the method used to analyze these dimmings and describe two test cases used to verify the robustness of our method. In § 3 we describe the spatial and temporal characteristics of the dimmings. In § 4 we conclude.

2. METHOD

2.1. *Data*

The data used in this study are from the *Solar and Heliospheric Observatory* (*SOHO*) EIT instrument (Delaboudiniere et al. 1995). We restrict our study to the 195 Å passband, which is the most commonly used filter. Images at this wavelength are generally taken at a 12 minute cadence and provide consistent coverage of most events. We include both full-resolution (2.6″ pixel^{-1}) and half-resolution images. We account for solar rotation by using a mapping technique, `drot_map.pro`, within Solarsoft (Freeland & Handy 1998) that is based on the solar differential rotation

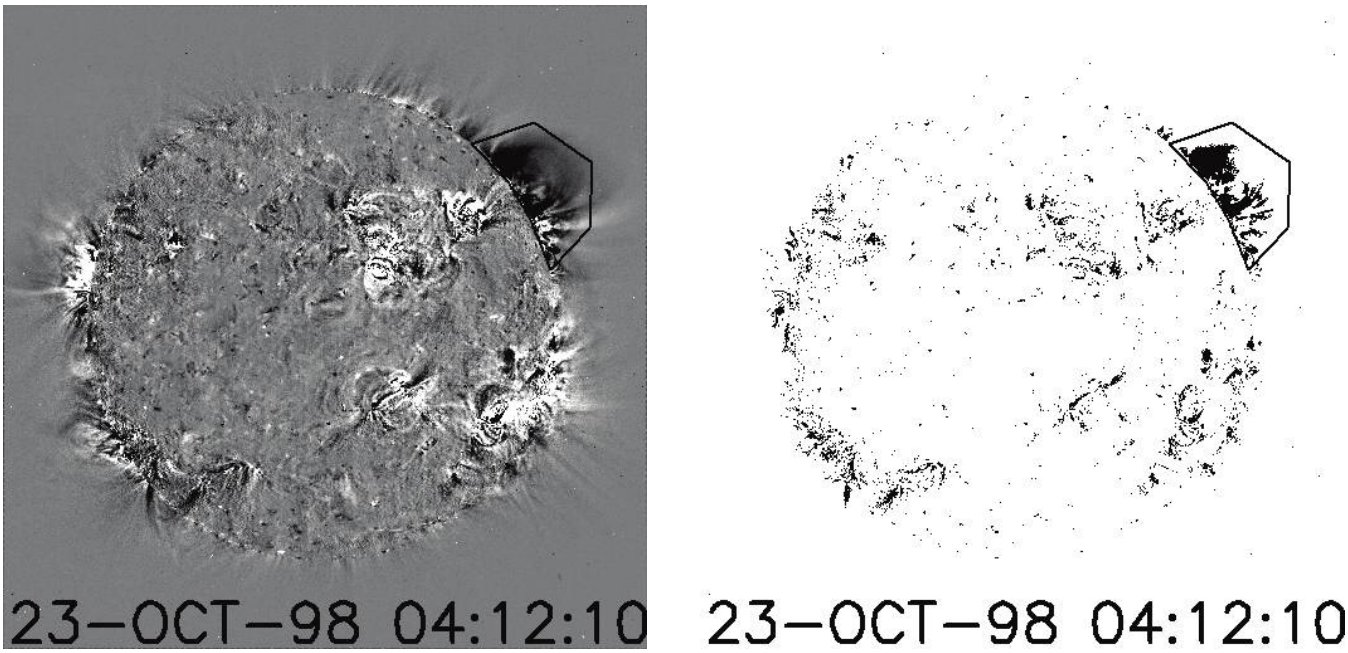

FIG. 1.—Example of a dimming event on the limb. In the left panel the difference image is shown. In the right panel only dim pixels are displayed.

formula of Howard et al. (1990). This technique is optimized for photospheric images and is somewhat less accurate for coronal wavelengths, but the results are sufficiently accurate for our analysis.

2.2. *Event Selection*

Dimmings were chosen based on lists compiled by the authors and others (B. Thompson 2006, private communication) of events over 3 yr in the rising phase of the solar cycle, from 1998 through 2000. In addition, a search was done for dimmings associated with all halo CMEs in the years 1998–2000. Of the 114 total halo CMEs listed in the CME database (Yashiro et al. 2004), we found clear dimmings associated with 30. If we assume that half of the halo CMEs (57) were frontside CMEs, we find 53% (30/57) of frontside CMEs have associated dimming events. This value is a lower limit given that some dimmings may not have been suitable for our study because of partial data gaps, low signal, etc. With a conservative estimate of more than 50% association, it is clear that dimming events are a significant aspect of the CME process.

For this study we focus on CME-associated dimmings, so our selection criterion requires that each dimming must occur in a location consistent with the associated CME and must begin within 4 hr before the CME is first seen in C2 and 2 hr after the first observations in C2, as defined by the *SOHO* LASCO CME

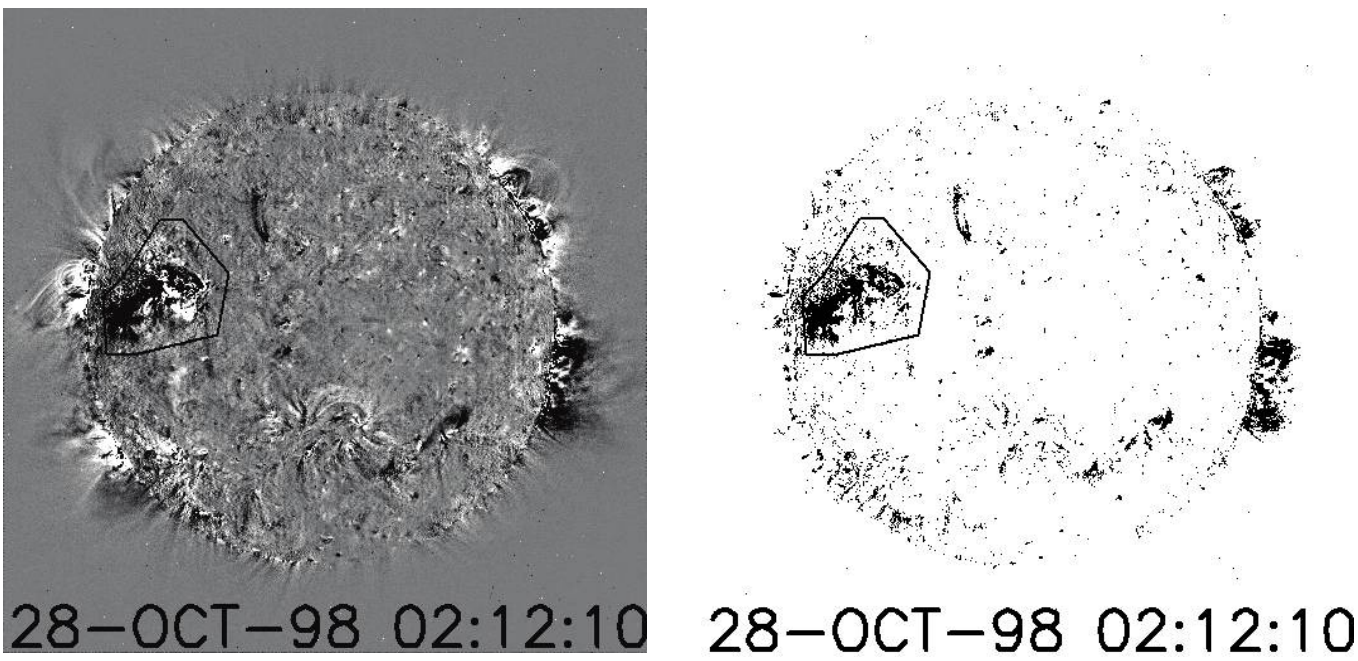

FIG. 2.—Example of a dimming event on the disk. Same format as Fig. 1.

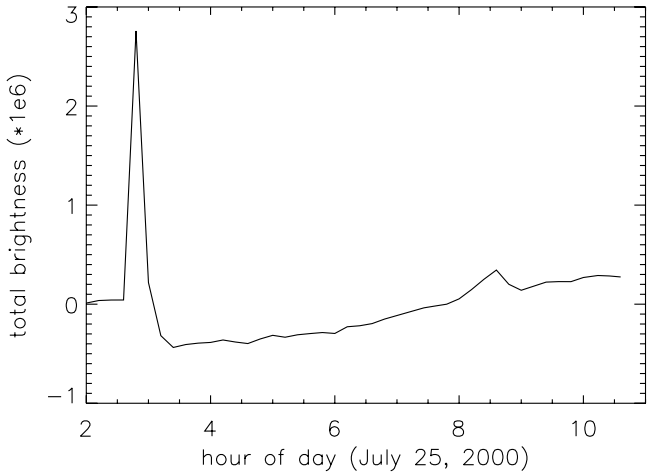

FIG. 3.—Total solar brightness within the dimming region on 2000 July 25. The flare at 02:30 obscures most of dimming event.

catalog (Yashiro et al. 2004[1]). Overall, we identify 96 dimmings, including 86 disk events and 10 limb events. This is not intended to be a complete catalog of dimmings, but rather a sufficient sampling of events for a statistical analysis. The mean time difference between the beginning of the dimming and the first observation of the associated CME in C2 is 1.39 ± 0.1 hr. The error bars used throughout this paper denote the uncertainty in the mean defined as $\sigma/\sqrt{n}$, where σ is the standard deviation and n is the number of events.

2.3. *Analysis Technique*

In order to characterize each dimming region we use difference images obtained by subtracting a pre-event frame from each event image. Then, for each dimming, a region is selected by hand that is large enough to include the dimming region at its maximum extent. The tool used to select the region allows the user to choose vertices that are then connected by straight lines. The user can select as many vertices as necessary in order to select a region that surrounds the dimming throughout the event. In cases where the dimming occurs within an active region we include the entire active region. The dimmings were followed for as long as they persisted or until rotation effects began to overwhelm the data (because of three-dimensional structures the derotation program was not able to perfectly account for rotation). Difference images displaying dimming events and the selected region are displayed in the left panels of Figures 1 and 2 for a limb dimming and a disk dimming, respectively.

To investigate the evolution of these dimmings we first define the area and brightness of each dimming. The simplest method would be to define the area as the total number of pixels within the selected region and to define the brightness as the sum of all pixels in the selected region. This method would be effective for well-behaved, regularly shaped dimmings. However, typical dimmings are irregular in shape and change in time, expanding or contracting. In addition, flares can overwhelm the data and nonflare brightenings within the active region can raise the overall brightness, skewing the results. To get an objective measure of the degree of dimming, we have developed a method that is less susceptible to these effects. We start by defining dim pixels as those pixels that are more than 1 σ below the mean value of the whole differenced image. This threshold was selected because of its effectiveness at revealing the dimming regions. The right-hand panels of Figures 1 and 2 display only the dim pixels.

This method of selecting for analysis only dim pixels within the hand-drawn region of interest greatly minimizes the influence of flares. Flares may still obscure part of the event, leading to a lower number of resulting dim pixels, but they will no longer overwhelm the data. For example, in Figure 3 we plot the sum of all pixels, or total brightness, within the selected region on 2000 July 25. In Figure 4 we plot the sum of only the dim pixels and the total number of dim pixels for the same event. The total brightness in Figure 3 is completely overwhelmed by a flare that occurs at 0230 hr, while the sum and number of dim pixels (Fig. 4) are minimally affected. Using this method, we now have two ways to look at the time history of a dimming event. A raw count of the number of dim pixels over time provides a view of how the *area* of the event changes with time, while the sum of the dim pixels represents the changes in *brightness* with time.

2.4. *Robustness of Analysis*

The selection of each dimming region is done by hand, and is thus potentially subjective. To test the robustness of the selection process we take one of our dimming events and select an optimal

[1] Available at http://cdaw.gsfc.nasa.gov/CME_list.

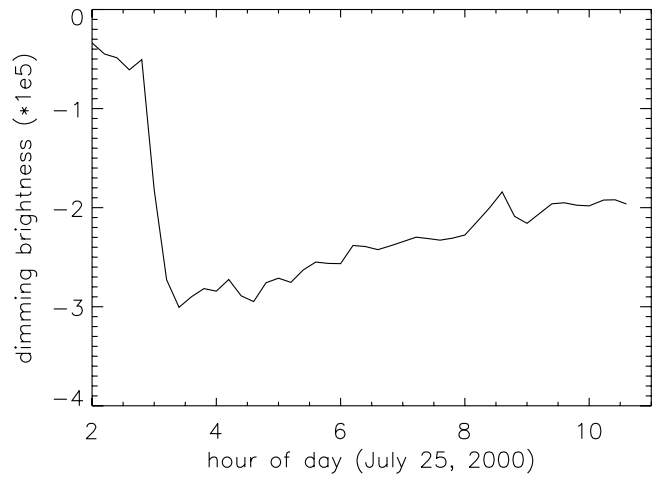

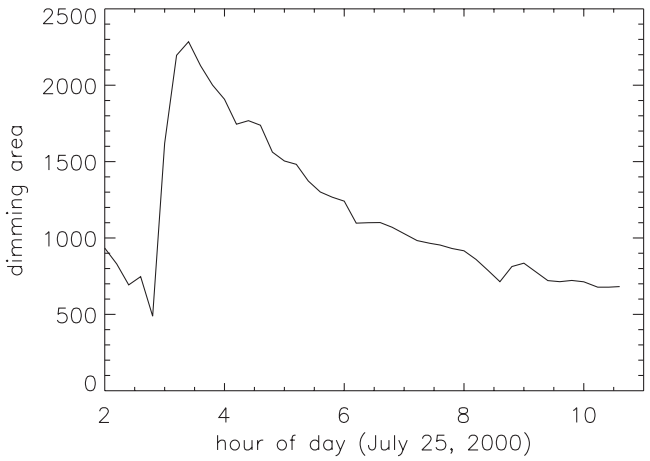

FIG. 4.—Sum of dim pixels (*left*) and total number of dim pixels (*right*) within the same event as Fig. 3. The flare at 02:30 causes a small artifact in each quantity, but these quantities are minimally affected by the flare, unlike the total solar brightness. We use this method to estimate the dimming brightness (sum of dim pixels) and area (total number of dim pixels).

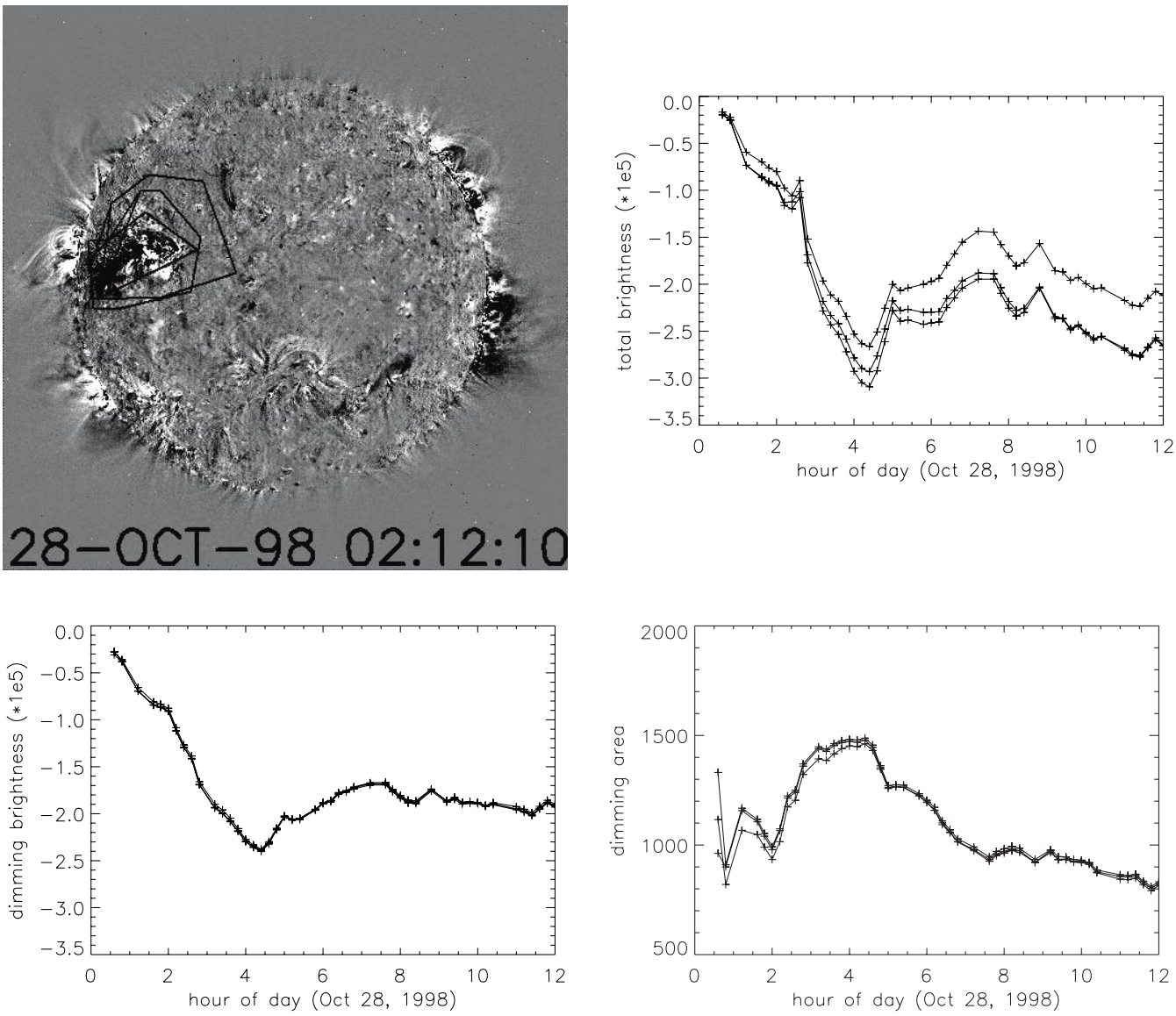

FIG. 5.—Different selected regions used to determine the effect of selected area on results (*top left*) and sum of all pixels (*top right*) and results based only on so-called dim pixels: sum of dim pixels (*bottom left*) and number of dim pixels (*bottom right*). Changing the size of the selected region has a large effect on total dim pixels, with larger selected regions having higher total intensities. However, the effect on the dim pixels is minimal.

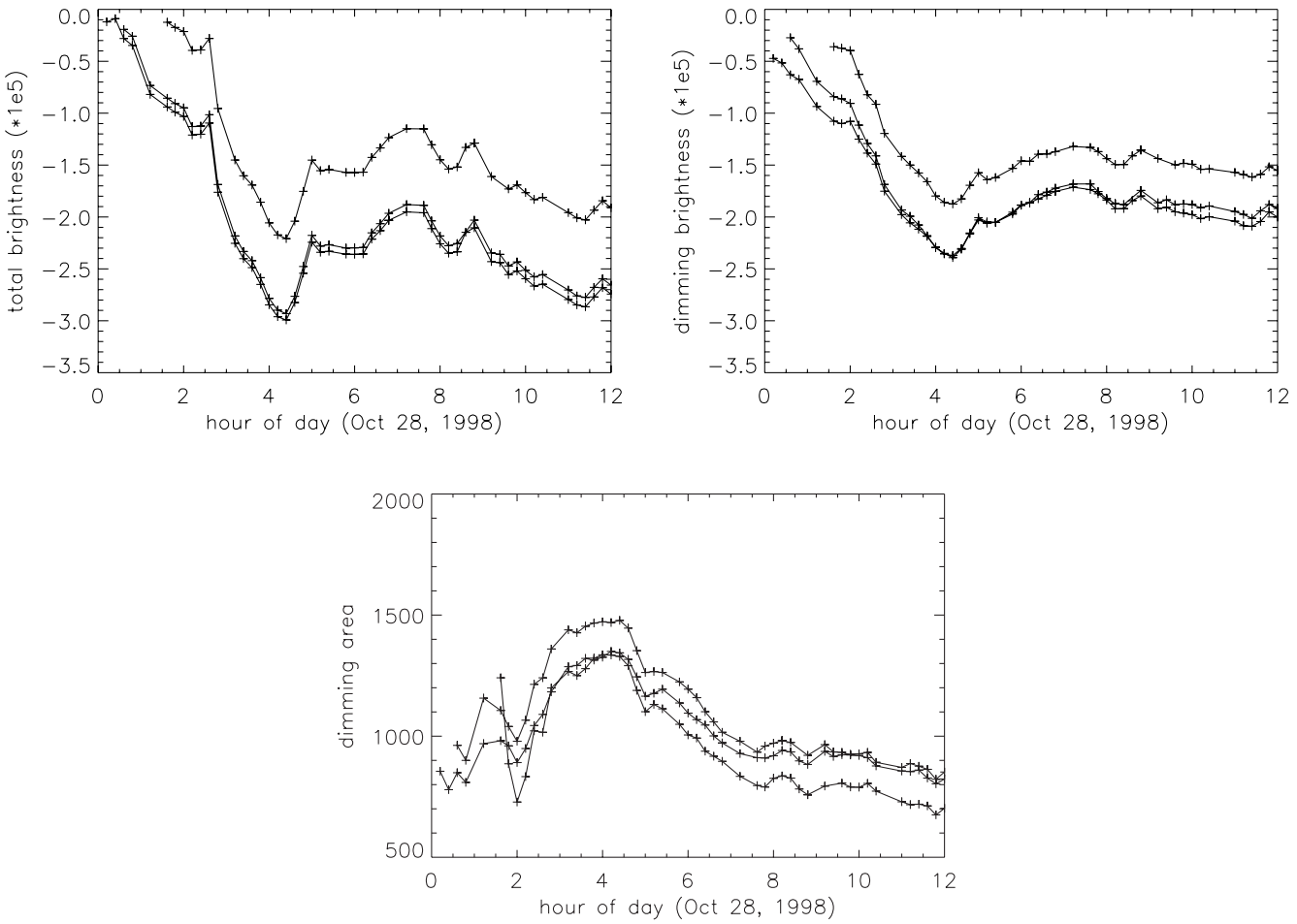

FIG. 6.—Effect of different reference images to measure the total brightness (*top left*), dim pixel brightness (*top right*), and dim pixel area (*bottom*). For total brightness, difference reference images can yield significant differences, particularly when the initial frame is chosen too late (*top curve*). For the dim pixel brightness the differences are similar. For the dim pixel area, the difference is minimal when the initial frame is taken too early, but there is a large effect when it is taken too late.

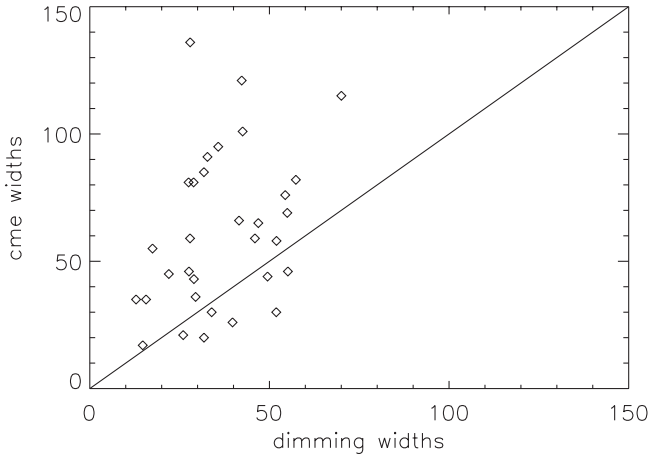

FIG. 7.—CME width vs. associated dimming width. The line denotes equal widths. Most CMEs are wider than their dimming counterpart.

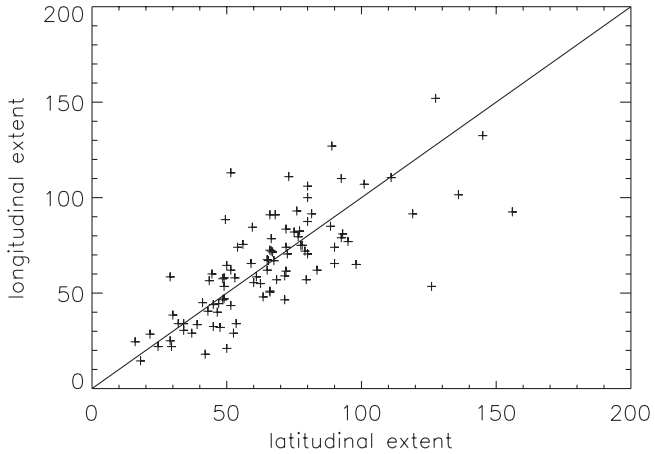

FIG. 8.—Extent in latitude vs. extent in longitude of each dimming region. These regions are fairly symmetric and range in size from small events of 18° on a side to large events extending over much of the solar disk. A line, constrained to intersect the origin, is fit through the data and is near unity with a slight tendency for the extent in latitude to be larger than the extent in longitude.

region as usual, as well as one larger and one smaller region, and compare the results. In Figure 5 the three regions are shown along with line plots of the total brightness, the dim brightness, and the dim area within the various regions over time. The total brightness is different for each of the three regions, with the largest region having the larger flux over time. The brighter ambient regions surrounding the dimming contribute to the total flux and increase the overall brightness of the dimming region. On the other hand, when we plot the sum of only those pixels that qualify as "dim" pixels, i.e., the dimming brightness, we find that selecting a larger or smaller region has a minimal effect on the results. Similarly, the total number of dim pixels, i.e., the dimming area, is also mostly unaffected by an oversized selected region, but can be affected by a region which is too small and misses a few dim pixels. Based on this result, we ensure for each event that we select a slightly oversized region.

A second potentially subjective factor in our analysis is our choice of the pre-event image. Care must be taken when choosing the pre-event image, as some subtle brightening can occur in the buildup to eruption. If the pre-event image is chosen during this buildup the dimming can be exaggerated. In addition, an initial frame chosen too late will artificially reduce the brightness of the dimming. To test how the choice of initial frame affects the data we run the process using the same selected region, but three different start points (for example, 0000, 0100, 0200 UT). In Figure 6 we plot the total brightness, dim pixel brightness, and dim pixel area with time for each choice of initial frame. We find that the total brightness is somewhat affected by whether the initial frame is moved earlier or later, with later initial frames having the greatest effect. The dimming brightness behaves similarly, with a slight difference for an earlier initial frame, but a noticeable increase when the initial frame is moved later. The same is true to a larger degree with the dimming area. Changing the selection of initial frame does have some effect on the results, particularly if the frame is chosen too late, but selecting an initial frame well before the start of the event reduces the effect of initial frame selection in the results.

In summary, we have tested this method and we find that it is more versatile than a raw brightness measurement. Further, we have investigated the possible subjective elements and developed procedures to minimize them. From this method we obtain a measure of the brightness and area of the dimming regions based on our definition of dim pixels, and this method will be used for the following analysis. The terms "area" and "brightness" will be used in the rest of the paper to refer to the dim pixel area and brightness, respectively.

3. RESULTS

3.1. *Spatial Scales*

The location and size of the dimming regions has the potential provide information about the location and mass of the CME events and so we first quantify these dimming characteristics. The width, position angle, longitude, and latitude are determined based on the selected region. Because of the patchy nature of dimming regions it is difficult to use the dim pixels themselves to define the extent of the region and so we use the location and extent of the hand-selected region. The P.A. and width of each region are defined as for CMEs: the central P.A. is defined as the angle in the plane of the sky at the mode center of the hand-selected region in polar coordinates, and the width is defined as the difference between the maximum and minimum P.A. of the dimming region. The widths ranged from 13° to 161° (excluding halos) with an average of 61° ± 4°. For a more direct comparison with the associated CMEs we consider only events within 30° of the solar limb. There were 31 events that met this criterion. The dimming widths ranged between 15° and 101° with a mean of 41° ± 4° and the associated CMEs had widths ranging from 17° to 196° with a mean of 70° ± 7°. Plotting these values together (Fig. 7), we find that the CME widths tended to be wider than the associated dimming width, suggesting that CME expansion occurs or that the dimming region selected does not account for the entire region which participates in the eruption. Note that

TABLE 1
COMPARISON BETWEEN CME AND DIMMING PLANE-OF-SKY WIDTH

Parameter	Dimming Regions	Associated CMEs	LASCO CMEs
Average width (P.A.).....	36° ± 13°	60° ± 30°	72°
Median width (P.A.).....	34°	58°	50°
Latitude range	S53° to N60°	S32° to N32°	S50° to N50° (1998)

NOTE.—Typical values of width and longitude for dimming regions, CMEs that are specifically associated with those regions, and for a list of 841 LASCO CMEs analyzed by St. Cyr et al. (2000).

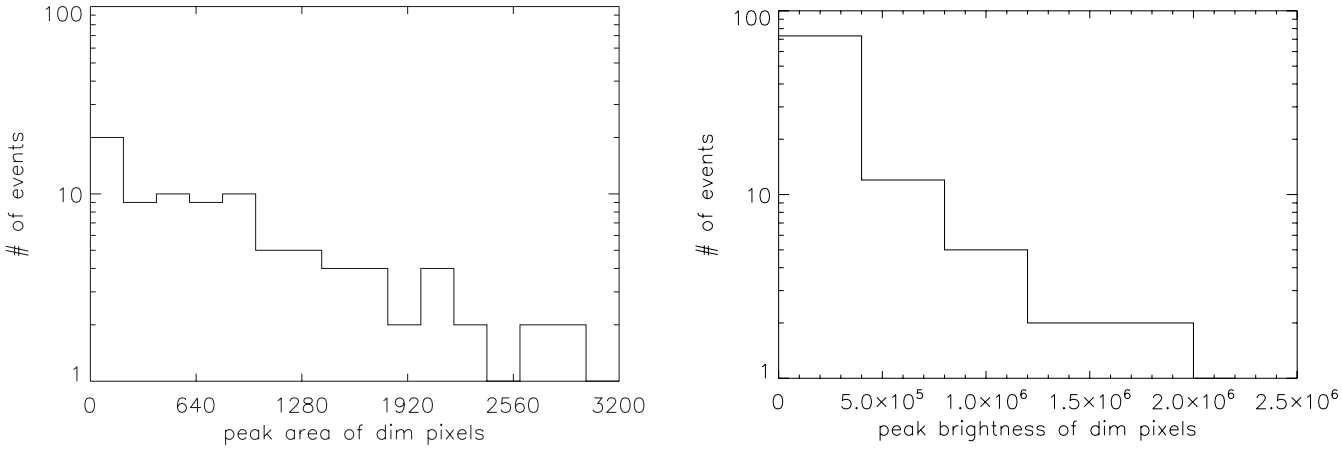

FIG. 9.—Peak total brightness and area vs. number of events. Data are exponentially distributed.

the selected region is generally larger than the dimming itself and so represents a maximum on the dimming size.

The longitudes and latitudes of each dimming were defined based on the location of the center of the selected region. The locations of the center point of the disk dimmings occur in typical active-region latitudes and at all longitudes, indicating no bias in the selection process. In overall extent on the disk, the dimming regions range from 15° to 152° in longitudinal width with an average extent of 65° ± 2.7° and 16° to 156° in latitudinal width with an average extent of 66° ± 2.7°. Again, these sizes are based on the selected region, and represent a maximum on the actual size of dimming regions. In addition, the sizes have not been corrected for the three-dimensional aspect, i.e., events near the limb may be small but subtend a large area. This effect is present for both latitude and longitude measurements, but has a slightly greater effect on longitude, as events near the north and south poles are relatively rare. The extent in latitude versus longitude for each event are plotted and fit to a straight line (constrained to go through the origin) in Figure 8. The events are symmetric, with the straight-line fit indicating that the average event has exactly the same extent in latitude and longitude. For comparison, St. Cyr et al. (2000) analyzed 841 LASCO CMEs and found an average apparent width of 72° and a median width of 50°. More than 50% of the St. Cyr et al. (2000) events had central latitudes within ±10° of the equator during 1996 and 1997, and the central latitudes extend to ∼50° in 1998. These values are compared to our results in Table 1.

3.2. *Time Histories*

We next investigate the temporal evolution of the dimming regions, to probe the dynamics involved. To simplify this discussion, we refer to the period of increasing area or decreasing brightness as the rise time, and the period of decreasing area or increasing brightness as the recovery time. The determination of dimming duration is somewhat subjective. We define the beginning, peak, and end of the dimming as follows in order to reduce that subjectivity. The beginning of the dimming is defined as two successive points of decreasing brightness or increasing area. The end of the dimming is determined by three successive flat points, with a decrease of less than 5% or an increase of less than 10%. The peak is defined as the point of maximum area occurring between the previously defined beginning and end of the dimming. The log values of the peak brightness and area of each event are shown in Figure 9 in histogram form. The dimming durations ranged from 1 to 19 hr with an average of 8.0 ± 0.4 hr and a median of 7.4 hr (Fig. 10). The majority of events last between 3 and 12 hr. The durations determined from the brightness and area are similar, but the time profiles vary. Inspection of Figures 4 and 5 reveals that the rise portion of the events occur over a shorter

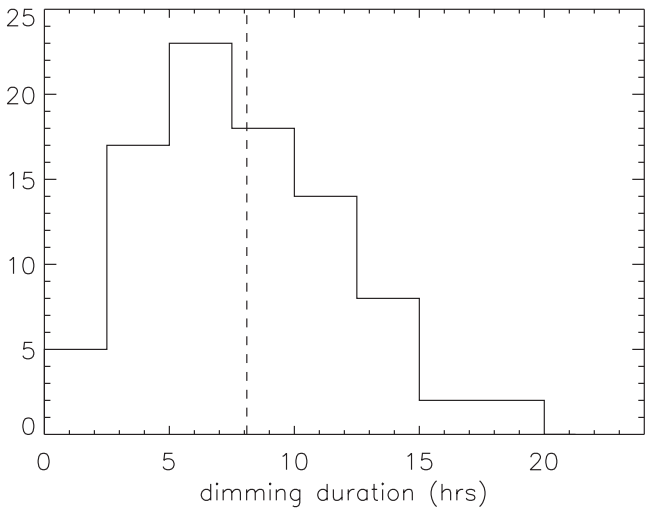

FIG. 10.—Distribution of dimming durations. The average duration is 7.8 hr, but a significant number last between 3 and 12 hr, with a few lasting as long as 22 hr.

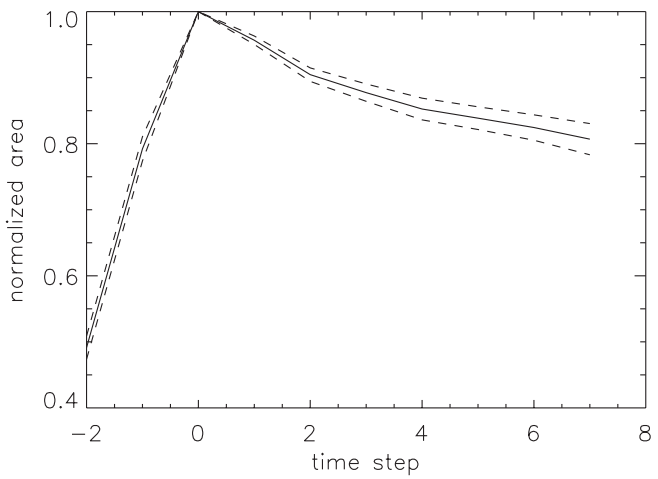

FIG. 11.—Superposed epoch analysis of all dimmings, aligned by the peak of each dimming. Characteristically, the dimmings have a sharp rise to maximum, followed by a slow decrease. The evidence of two-part slopes can be seen here.

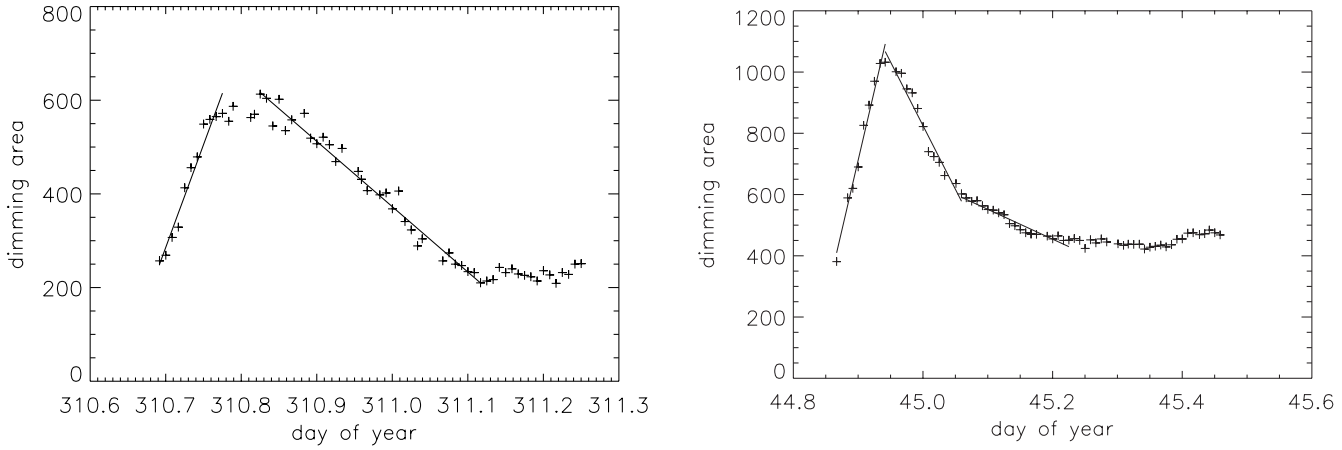

FIG. 12.—Examples of dimmings with a single-component decay (*left*) and two-part decay (*right*). For the simple component decay, the slope during the rise portion is typically much steeper than during the recovery period, whereas for events with a two-part decay the initial decay period has a similar slope to the rise period, followed by a second, more gradual decay.

timescale than the recovery portion. To quantify this, we fit the rise and decay slopes of both the area (number) and brightness (sum) of the dim pixels. We find that the area has a slightly shorter rise time than the brightness (3.25 ± 0.25 hr vs. 3.6 ± 0.3 hr) and a longer recovery time (4.8 ± 0.3 hr vs. 4.3 ± 0.3 hr), indicating that the dimmings reach their maximum size and then continue to deepen. In both area and brightness, the rise times are shorter than the recovery times. The variations between events are large (standard deviations are nearly 3 hr each), but the number of events allows a more precise determination of the average event.

To determine how an "average" dimming event would appear, we conduct a superposed epoch analysis (Fig. 11). This process involves dividing each event into 10 intervals and averaging the data points within each interval. This analysis basically compresses each dimming to the same length so that the time profiles can be averaged together to yield an average dimming. The beginning and peak of each event are determined as described in the paragraph above. We define the interval between the beginning of the event and the peak of the event as 3 time steps. We follow the dimmings for seven more time steps (e.g., if the beginning of the event is at 0200 and the peak is at 0220, we define a time step as 10 minutes and follow the dimming until 0330). The peak of each event is normalized to a value of 1, so that larger events do not dominate the average. The error bars indicate the uncertainty in the mean for each time step. The result illustrates the typical sharp increase to maximum dimming, followed by the slow recovery. We note that the dimmings frequently do not recover to pre-event values. This effect is largely due to darkening caused by the rotation of three-dimensional objects. There is evidence of a two-part recovery slope in the average dimming.

Investigating the recovery phase of these events further, we find that about 76% of the brightness and 72% of the area time series could be well fit with a single recovery slope, but the remaining events had a two-part slope (see Fig. 12 for two examples). The character of the two-part slope was similar for area and brightness with a steep initial recovery slope lasting 3.3 ± 0.3 hr (3.6 ± 0.3 hr) followed by a flatter recovery lasting 4.8 ± 0.3 hr (4.3 ± 0.3 hr) for the area (brightness). This two-part slope may provide some insight into the dimming recovery method, with

TABLE 2
SUMMARY OF RISE AND RECOVERY VALUES FOR THE DIMMING AREA AND BRIGHTNESS

Parameter	Area	Brightness
One-part rise time (hr)	3.3 ± 0.3	3.6 ± 0.6
Recovery time (hr)	4.8 ± 0.3	4.3 ± 0.3
Two-part recovery	72%	76%
Rise time (hr)	2.2 ± 0.2	2.6 ± 0.3
Initial recovery time (hr)	3.2 ± 0.4	3.0 ± 0.4
Secondary recovery time (hr)	3.8 ± 0.5	3.6 ± 0.6

NOTE.—Simple, one-part recovery slopes are summarized in the first two rows, while events with a two-part recovery process are summarized in the last four rows.

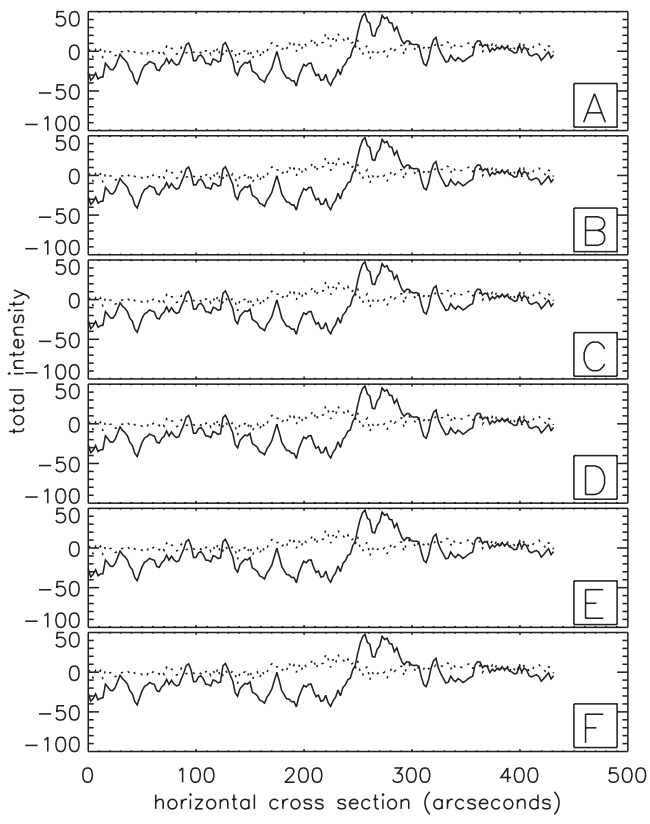

FIG. 13.—Cross sections of the dimming event shown in Fig. 14. Lettered panels match the images in Fig. 14.

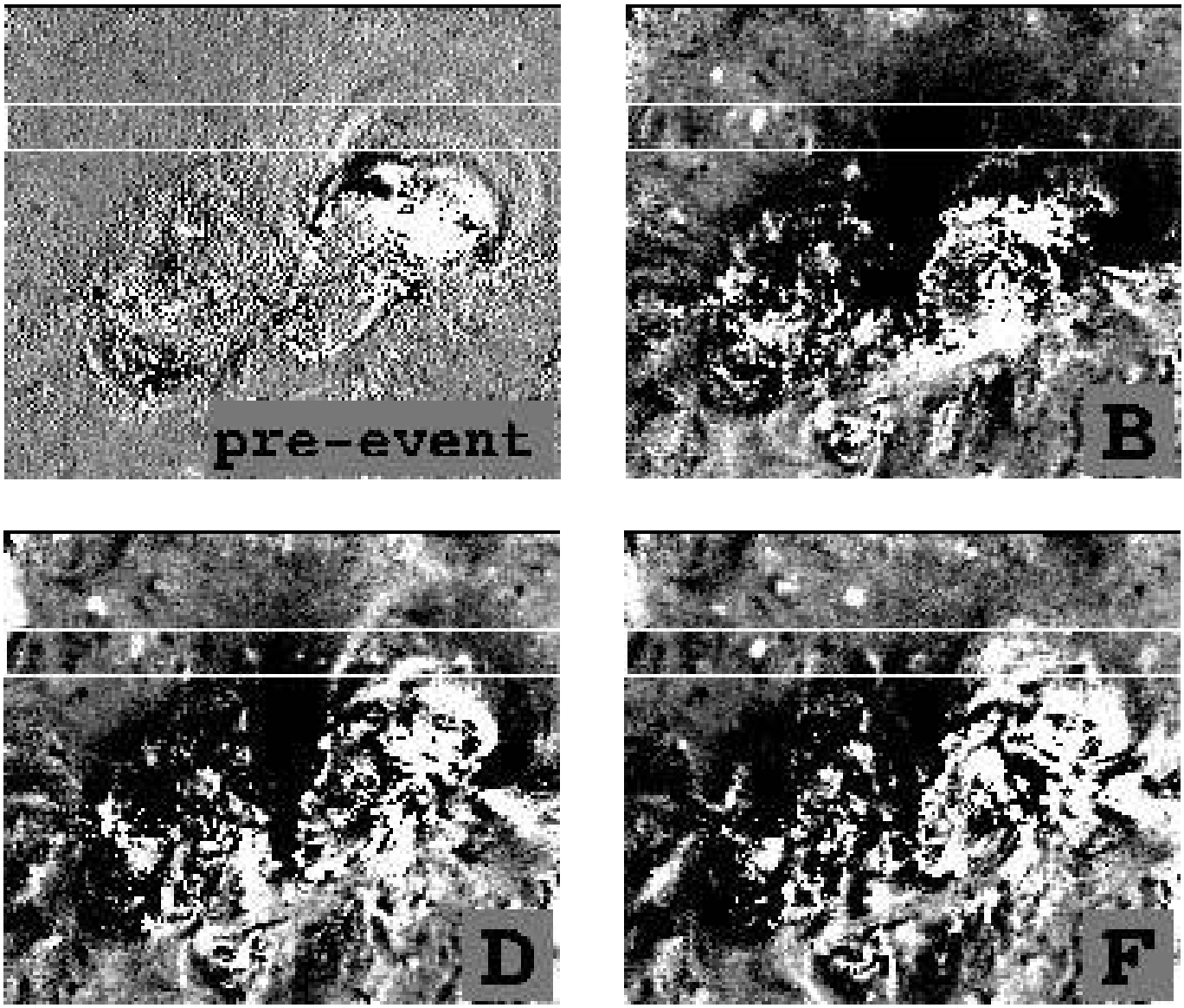

FIG. 14.—Time sequence of dimming event selected images from Fig. 13.

some faster inflow of plasma followed by a slower inflow. The initial recovery time is similar in magnitude to the dimming rise slopes quoted above, perhaps indicating some similarity between how the plasma is removed and initially restored. These values are summarized in Table 2.

To examine a specific example of the spatial evolution of dimming regions we take the cross section of a dimming at regular intervals through the event (Figs. 13 and 14). The images associated with selected frames of Figure 13 are shown in Figure 14. The cross section for a background subtracted pre-event image (on the top left of Fig. 14) is shown in each frame of Figure 13 as the dotted line. By frame A of Figure 13 the area has already reached its maximum extent, ranging 180″ (from 120″ to 400″ in the figure). The brightness is seen to deepen further in frame B. This observation can also be seen in the cross section of the image in Figure 14 also labeled B. By frame C both the area and brightness have reached their maximum extent and begin to recover. Between the frames D and F the selected area slowly recovers to the pre-event level. As seen in Figure 14 the recovery is near complete in the selected cross section by frame F (although the dimming is still present in the frame).

4. CONCLUSIONS

We report on a statistical study of 96 coronal dimmings observed with EIT on the solar disk from 1998 to 2000. Of these events, 86 were visible on the disk and 10 were limb events. The angular widths of these dimming regions averaged 41°, which is significantly smaller than typical CME values between 60° and 72°. The dimmings lasted between 1 and 19 hr and tended to quickly reach a maximum and then slowly recover, sometimes with a two-part slope. The total number of dim pixels (representing the area of the dimming) was slightly more likely to recover with a two-part slope, while the sum of the dim pixels (representing the brightness of the dimming) was more likely to recover with a single slope.

These results provide a starting point for a full understanding of dimming regions and their relationship to the origin and evolution of CMEs. Further analysis will compare these dimming regions directly to the associated CME properties. Results have the potential to connect low coronal activity more directly with upper corona manifestations of CMEs and improve the power of coronal dimming regions to predict associated CME quantities.

REFERENCES

Delaboudiniere, J.-P., et al. 1995, Sol. Phys., 162, 291
Freeland, S. L., & Handy, B. N. 1998, Sol. Phys., 182, 497
Gopalswamy, N., & Hanaoka, Y. 1998, ApJ, 498, L179
Hansen, R. T., Garcia, C. J., Hansen, S. F., & Yasukawa, E. 1974, PASP, 86, 500
Harra, L. K., & Sterling, A. C. 2001, ApJ, 561, L215
Harrison, R. A., Bryans, P., Simnett, G. M., & Lyons, M. 2003, A&A, 400, 1071
Harrison, R. A., & Lyons, M. 2000, A&A, 358, 1097
Howard, R. F., Harvey, J. W., & Forgach, S. 1990, Sol. Phys., 130, 295
Hudson, H. S., Lemen, J. R., St. Cyr, O. C., Sterling, A. C., & Webb, D. F. 1998, Geophys. Res. Lett., 25, 2481
Hudson, H. S., & Webb, D. F. 1997, in Coronal Mass Ejections, ed. N. Crooker, J. Joselyn, & J. Feynman (Geophys. Monogr. 99; Washington: AGU), 27
Kahler, S. W., & Hudson 2001, H. S., J. Geophys. Res., 106, A12, 29239
Podladchikova, O., & Berghmans, D. 2005, Sol. Phys., 228, 265
Rust, D. M., & Hildner, E. 1976, Sol. Phys., 48, 381
St. Cyr, O. C., et al. 2000, J. Geophys. Res., 105, 18169
Sterling, A. C., & Hudson, H. S. 1997, ApJ, 491, L55
Stewart, R. T., & McCabe, M. 1974, Sol. Phys., 36, 203
Thompson, B. J., Cliver, E. W., Nitta, N., Delannee, C., & Delaboudiniere, J.-P. 2000, Geophys. Res. Lett., 27, 1431
Thompson, B. J., et al. 1999, ApJ, 517, L151
Yashiro, S., Gopalswamy, N., Michalek, G., St. Cyr, O. C., Plunkett, S. P., Rich, N. P., & Howard, R. A. 2004, J. Geophys. Res., 109, A07105, DOI: 10.1029/2003JA010282
Zarro, D. M., Sterling, A. C., Thompson, B. J., Hudson, H. S., & Nitta, N. 1999, ApJ, 520, L139